

Article

Numerical Investigation of the Seismic Performance of an Innovative Type of Buckling-Restrained Brace (BRB)

Ali Naghshineh ^{1,*}, Oliver Fischer ¹, Nasreen B. Pathan ², Logan Couch ² and Fariborz M. Tehrani ² 

¹ School of Engineering and Design, Concrete and Masonry Structures, Technical University of Munich (TUM), 80290 Munich, Germany

² Department of Civil & Geomatics Engineering, California State University, Fresno, CA 93740, USA

* Correspondence: a.naghshineh@tum.de

Abstract: Previous studies have demonstrated that the inclusion of tire-derived aggregate (TDA) enhances the damping, ductility, and toughness of concrete mixtures. The effectiveness of tire-derived aggregate as a ductile material with a higher damping ratio and lower density in buckling-restrained braces has been examined at California State University's Structures Laboratory (CSU). Through experimental and theoretical investigations, this study compares the structural application of buckling-restrained braces with TDA and with conventional concrete infill subjected to various ground motions as well as artificial excitations. The evaluations include modeling a full-scale experimental setup equipped with a single-leg BRB utilizing ETABS 2016 and OpenSees 2000 software. The effectiveness of the application is demonstrated through a comparison of accelerations, displacements, stiffness, and damping ratios between TDA and concrete filling. Additionally, a design guideline for TDA-filled buckling-restrained braced frames is provided.

Keywords: tire-derived aggregate; seismic performance; experimental; steel frame; buckling-restrained braced frame; ductility; toughness; passive control; dynamic response



Citation: Naghshineh, A.; Fischer, O.; Pathan, N.B.; Couch, L.; Tehrani, F.M. Numerical Investigation of the Seismic Performance of an Innovative Type of Buckling-Restrained Brace (BRB). *Eng* **2023**, *4*, 2978–2990. <https://doi.org/10.3390/eng4040167>

Academic Editor: Alessio Cascardi

Received: 14 September 2023

Revised: 25 October 2023

Accepted: 22 November 2023

Published: 1 December 2023



Copyright: © 2023 by the authors. Licensee MDPI, Basel, Switzerland. This article is an open access article distributed under the terms and conditions of the Creative Commons Attribution (CC BY) license (<https://creativecommons.org/licenses/by/4.0/>).

1. Introduction

Buckling-restrained braced frames (BRBFs) offer an alternative to conventional braced frames, which have displayed poor performance during past earthquakes, including buckling failure, limited ductility, fracture in connections, and asymmetric hysteresis behavior. A typical BRBF consists of a ductile steel core embedded in concrete and encased concrete in a steel tube to prevent brittle failure modes.

This study explores the potential of modified concrete using waste tire chips that has a lower strength and stiffness yet a high toughness. However, when its strength falls too low, it becomes unsuitable for construction. The potential for increased strength and stiffness at a reduced cost by substituting waste tires in the form of fibers instead of chips was investigated [1]. A total of 42 cylinders underwent testing for compressive strength, split tensile strength, and modulus of elasticity. Twelve cylinders were prepared with waste tire chips, while thirty specimens were constructed using waste tire fibers, varying in terms of length and stiffness. The results indicated that using waste tire fibers in modified concrete as opposed to waste tire chips leads to increased stiffness and strength. Moreover, analytical studies confirmed that waste tire fibers could also reduce stress concentrations. Further studies, such as beam fatigue tests, are necessary to evaluate the practical use of rubberized concrete in constructions. Rubberized concrete showed an improved heat transfer, but reduced sound absorption compared to standard concrete [2]. Testing involved 64 specimens with varying levels of crumb rubber as a fine aggregate replacement. The results showed a decreased compressive and tensile strength, improved sound absorption, and higher electrical resistivity in crumb rubber-modified blocks.

Aslani [3] investigated the effects of rubber types and content on various properties including compressive strength, tensile strength, flexural strength, modulus of elasticity,

strain, and stress–strain curves. The investigation of large-size TDA material showed that the unit weight of TDA depends on placement and compaction [4]. A whole yield and the secant friction angles of 24 and 60 were set as the upper bound and lower bound, respectively. The low unit weight of these materials makes them suitable for landslide repair and weak foundation soils. The shear behavior tests of TDA with large-size particles were performed, and the related properties and interface shear strength against concrete were measured [5]. The internal failure was nonlinear, with a decreasing peak secant friction angle from 39.6 to 30.2. In contrast, the TDA–concrete interface failure exhibited linear failure, with a higher initial shear stiffness than the TDA’s internal shear test. Rubberized concrete exhibits a superior impact resistance and enhanced damping properties for cost-effective and flexible concrete barriers, in contrast to conventional concrete. However, increased tire chips decrease the compressive strength while improving energy absorption [6–11]. The impact of crumb rubber concrete on the ductility of profiled steel sheeting in composite slabs was also examined to achieve the desired performance [12].

The ductility and energy absorption capacity of RC columns by incorporating concrete waste tire rubber with varying compressive strengths, tire rubber size, and content were investigated [13]. Twelve column specimens were tested using two types of concrete with a compressive strength of 24 and 28 MPa and two different crumb rubber particle sizes (0.6 and 1 mm). The results indicated a reduction in the modulus of elasticity, compressive strength, and compressive load capacity when using waste tire rubber in concrete. Moreover, the lateral deformations and the energy dissipation capacity of column specimens utilizing waste tire rubber concrete were double those of the conventional concrete specimens. In addition, the curvature ductility increased to 45–90% with the inclusion of 0.5–1% waste tire particles in concrete mixtures. Other published research on rubberized concrete reported similar characteristics when incorporating rubber content in concrete mixtures. Increasing the rubber content resulted in decreased flexural and compression strengths but increased ductility, damping, toughness, sound isolation, and reduced density [14,15]. Therefore, the application of ductile materials with improved damping properties, such as tire-derived lightweight aggregate concrete, can further enhance the overall performance of the system.

In contrast to concrete, rubber is significantly softer and can tolerate far more deformation before failing. Crumb rubber consists of smaller particles, while tire chips are larger rubber particles used to replace fine and coarse aggregate in concrete [16]. The stress–strain curve of rubber is nonlinear, initially exhibiting a lower stiffness before increasing, while cement paste/mortars demonstrate brittle behavior with a higher compressive strength compared to tensile/flexural strength, following a linear stress–strain curve. Additionally, the inclusion of rubber-based aggregates results in decreased mechanical parameters, like compressive strength, tensile strength, flexural strength, and modulus of elasticity. Consequently, concrete containing a substantial proportion of rubber aggregate exhibited enhanced ductility compared to conventional concrete [17–22].

In the present study, the application of an innovative single-leg BRB with TDA and concrete infill is verified against the experimental tests conducted at the Structures Laboratory of California State University (CSU), Fresno. Based on the experimental tests, four models for a BRB with TDA and concrete filling are developed using ETABS and OpenSees software [23,24]. The models are subjected to various artificial loadings, including harmonic, periodic, and impulse loadings, as well as different ground motion loadings. The results allow for a comparison between the experimental and analytical studies, covering the acceleration, displacement, stiffness, and damping ratios of BRBs with TDA and concrete infill.

2. Tire-Derived Aggregate (TDA)

Tire-derived aggregate is derived from scrap tires accessible in a standard range of practical sizes. TDA is classified into two types, Type A (75–100 mm) and Type B

(150–300 mm) [25]. The mechanical properties from two experimental investigations are employed in the numerical simulations.

In the experimental study on tire-derived lightweight aggregate (TDLWA), the mechanical properties, including the compressive, splitting tensile, flexural strength, and flexural toughness, and an impact flexure test of rubberized lightweight aggregate, were investigated using 38 cylindrical and 36 beam specimens [26]. A target strength of 21 MPa was specified, and the cylinder and beam specimens were composed of shale lightweight coarse aggregate, natural sand fine aggregate, cement, and water. The TDA was then incorporated into the cylinder and beam specimens via a replacement with replacement ratios ranging from 0% to 100%. It was concluded that as the rubber content increased, the static mechanical strength decreased, while the ductility and toughness increased. Hence, these materials were found to be functional, particularly when energy absorption was a critical aspect. Nevertheless, dynamic testing was limited, and further comprehensive testing, both full-scale and small-scale, is warranted to gather more practical data.

The mechanical properties for TDA and concrete were conducted using six cylindrical specimens (0.1 m × 0.2 m) in accordance with ASTM C39 and C78, and ASTM C496 standards [27]. The test included compression and split tensile tests, with loads applied at rates of 0.24 MPa per second for compression and 48.9 kN per second for tensile testing. The test results for the concrete and TDA cylinders are presented in Table 1.

Table 1. Cylinder test results for concrete and TDA [27].

Cylinder Testing	Compression Strength	Cylinder Testing
Conventional concrete	34.6	11.2
TDA concrete	10.6	0.36

3. Buckling-Restrained Braces

Conventional steel-braced frames are used for lateral load resistance but have shown poor performance in past earthquakes due to factors like limited ductility and connection fractures. An alternative, buckling-restrained braces (BRBs), consist of a ductile steel core encased in concrete, providing the necessary yielding mechanism and the potential for enhanced seismic resistance. Buckling-restrained braced frames (BRBFs) can be categorized as one of the new types of seismic force-resisting systems, with the two primary bracing configurations being single-leg and concentrically braced frames. While a BRBF shares some geometric similarities with a conventional CBF, it exhibits noticeable distinctions in terms of connections, members, hysteresis behavior, and ductility. Figure 1 presents the BRBF details [28–30].

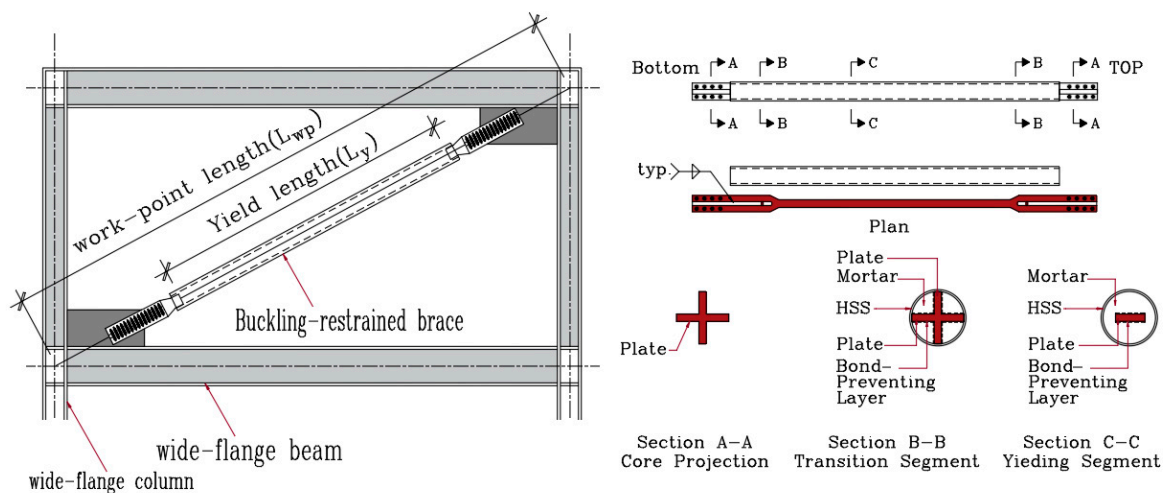


Figure 1. Single-leg buckling-restrained bracing and details [28–31].

The primary aim of this study is to demonstrate TDA's effectiveness as a filling material in comparison to conventional concrete filling. Figure 2 provides the specifics of the experimental buckling-restrained brace, with an effective length of 2.31 m (7'-7.0") and a total length of 2.51 m (8'-3.0"). The steel core cross-section, consisting of an A36 plate measuring 6.23 cm in × 0.32 cm (2.45 in × 0.125 in), is designed to withstand a lateral load of 27.7 kN.

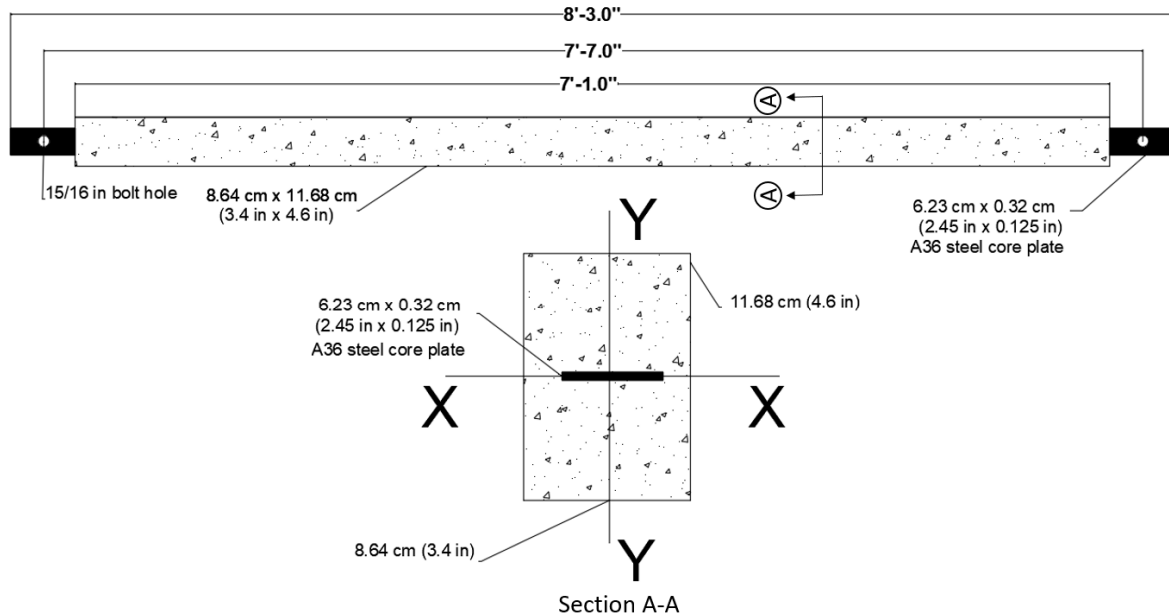


Figure 2. The experimental model of buckling-restrained brace [30].

The initial stiffness (K_{in}) of the buckling-restrained brace for both the TDA and concrete fillings is determined using Equation (1), utilizing the experimental results. In this equation, A_{sc} represents the steel core, E stands for the modulus of elasticity, and L_{wp} is the work point length, which can be predicated assuming minor angle changes. The axial deformation, Δ_{bx} , is calculated as the product of the drift angle, q_x , and the work point length, L_{wp} , multiplied by $\sin(2\alpha)$, where α represents the BRB angle. Subsequently, the yield length ratio is computed by dividing the length of the yielding region, L_y , by the work point length, L_{wp} . The initial stiffness is established based on the modulus of elasticity of the steel core (A36) [32], resulting in a value of 71.255 kip/in for both the BRB with TDA and concrete fillings.

$$k_{in} = \frac{A_{sc}E}{L_{wp}} \tag{1}$$

4. Experimental Setup

The setup consists of one bay in the X direction with a 2.02 m span length and two bays in the Y direction, each spanning 0.762 m. The frame has a height of 2.44 m and utilizes $W6 \times 9$ and $W6 \times 15$ (A992) for the columns and beams. Two concrete blocks, each weighing 1035 Kg, are placed atop the frame. Lateral translation is controlled by two wires with a 4.4 kN capacity, and the shake table measures 2.44 m × 2.06 m in the X and Y directions. Three accelerometers were employed to measure the frame vibrations, located at the northeast, southwest, and base of the frame (Figure 3).

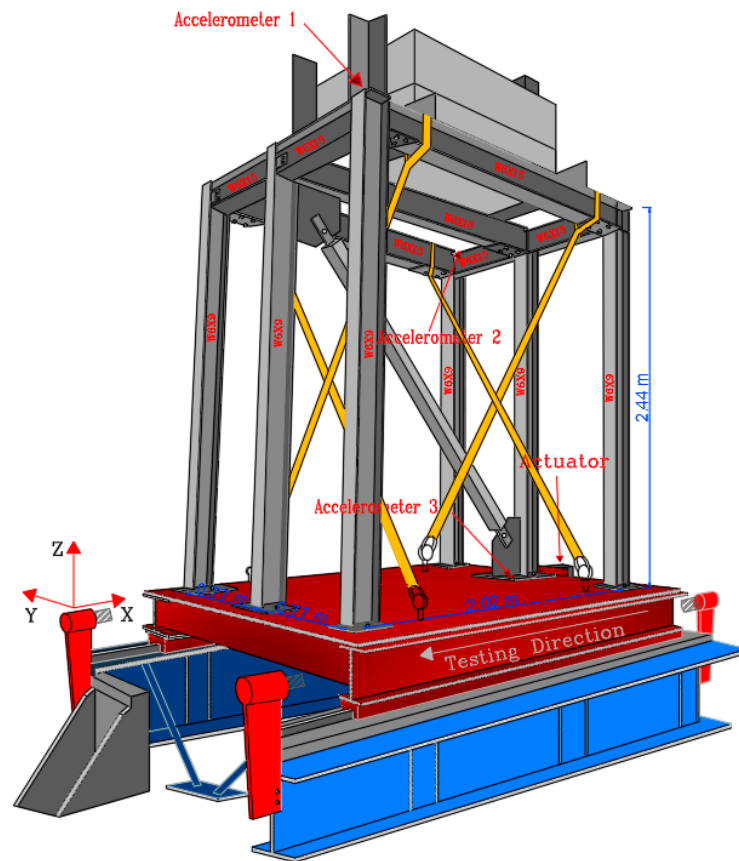


Figure 3. A 3-D and elevation view of the frame [30].

5. Loadings

The selected excitations were acquired from the Pacific Earthquake Engineering Research (PEER) database [33]. The scaling of ground motions was restricted to the base displacement of 12.17 cm (5") due to the limitations of the shake table. The frame was subjected to increasing amplitude FEMA loadings [34] with varying time steps (0.00625 s, 0.003125 s, 0.0125 s) and with maximum displacements of 20.32 mm (0.80") and 40.46 mm (1.60") in FEMA-2D. The analysis also included a 5 mm (0.2") frequency-increasing sweep loading and impulse loading, as presented in Figures 4 and 5 [30].

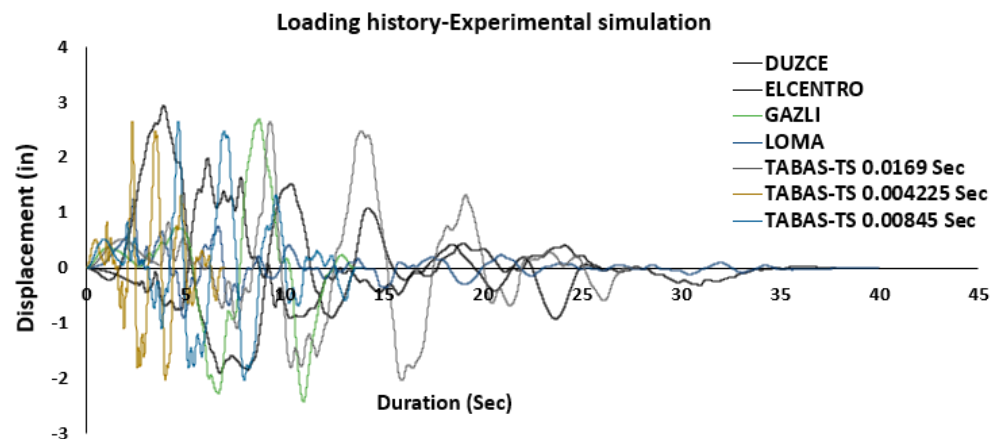


Figure 4. Ground motion loadings history [33].

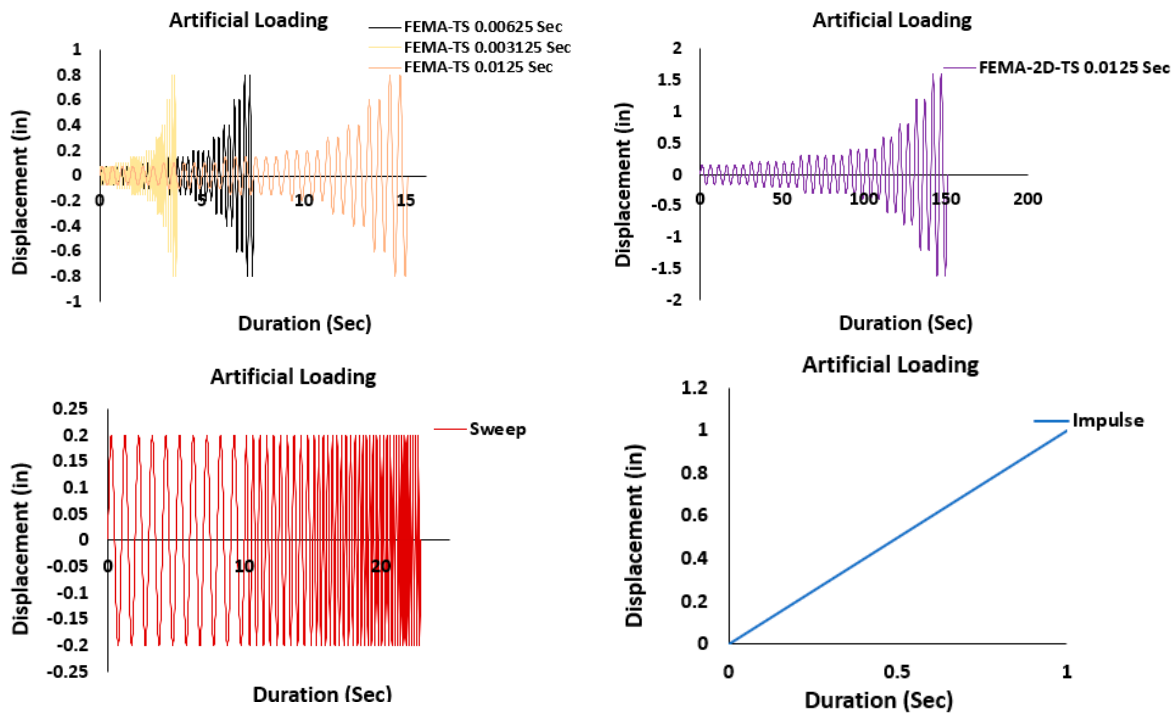


Figure 5. Artificial loadings history [30].

The time steps for each loading are calculated according to ASCE 41-17 [35] and FEMA P-2208 revisions [36]; these values are tabulated in Table 2.

Table 2. Selected time steps for acceleration and displacement.

Loadings	T_S (s)	$T/100$ (s)	T_{90} (s)	Selected T_S -Acceleration (s) (Min: $^1 T_S, T/100, T_{90}$, and 0.01_s)	Selected T_S -Displacement (s)
DUZCE	0.0050	0.0023	0.145	0.0023	0.0050
ELCENTRO	0.0050	0.0023	0.145	0.0023	0.0050
GAZLI	0.0066	0.0023	0.145	0.0023	0.0066
LOMA	0.0050	0.0023	0.145	0.0023	0.0050
TABAS 1	0.0169	0.0023	0.145	0.0023	0.0169
TABAS 2	0.004225	0.0023	0.145	0.0023	0.0042
TABAS 3	0.00845	0.0023	0.145	0.0023	0.0084
FEMA 1	0.00625	0.0023	0.145	0.0023	0.0062
FEMA 2	0.003125	0.0023	0.145	0.0023	0.0031
FEMA 3	0.0125	0.0023	0.145	0.0023	0.0125
FEMA-2D-4	0.0125	0.0023	0.145	0.0023	0.0125
Sweep	0.0125	0.0023	0.145	0.0023	0.0125

¹ T is the fundamental period of the structure, and T_{90} is the highest mode when T reaches 90% of modal mass participation.

6. Simulation of Experimental Model

Four numerical models were developed based on the experimental tests using ETABS and OpenSees software [23,24]. The weight of the existing blocks is applied as two-point loads, each with a magnitude of 2.3 kip (10.21 kN) on the middle beam (2-L1&L2) and four-point loads, each with a magnitude of 1.15 kip (5.1 kN) on the outer beams (1&3-L1&L2).

OpenSees is open-source, object-oriented software designed for earthquake engineering. It can be used to simulate structural responses through finite element computer applications [37–40]. The simulated experimental BRB frame with both TDA and concrete is depicted in Figure 6.

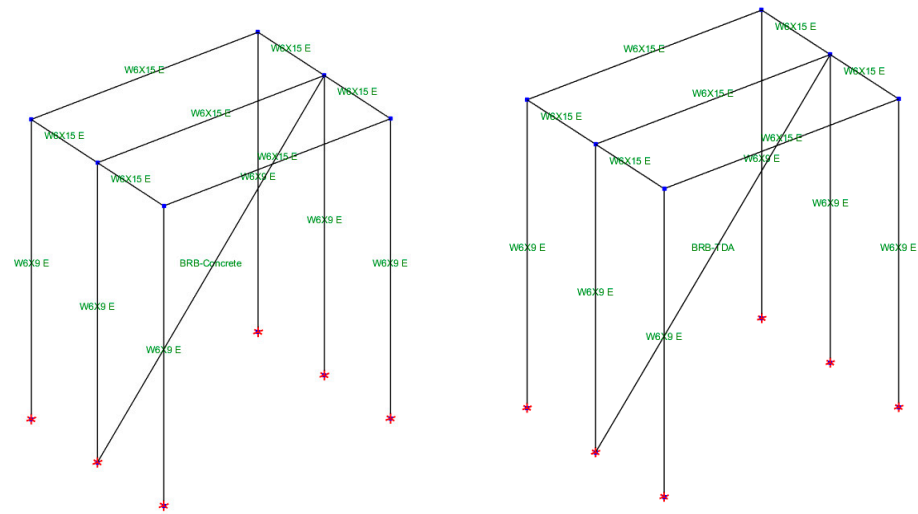


Figure 6. Simulation of experimental BRB frame using OpenSees software.

7. Results and Discussions

Selected roof acceleration–time diagrams for the BRB with concrete and TDA fillings, based on the experimental findings in the tension, compression, and an average of the tension and compression along with the analytical results from ETABS and OpenSees software [23,24], are presented in Figure 7 (concrete filling) and Figure 8 (TDA). All diagrams demonstrate a strong agreement between the experimental and analytical results. Figure 9 displays the maximum roof acceleration outcomes for the BRB with TDA and concrete fillings. The highest roof acceleration for the BRB with concrete infill was observed during the Loma Prieta ground motion, with a maximum of 0.49 g in the tension, 0.44 g in the compression, and an average acceleration of 0.46 g (experimental) and 0.42 g (simulation). For the frame subjected to the El Centro ground motion for the BRB with concrete infill, the minimum acceleration recorded was 0.24 g in the tension and 0.25 g in the compression, with an average acceleration of 0.245 g in the experimental study and a similar value of 0.23 g for the analytical work. In the case of the BRB with TDA filling, Tabas (TS-0.004225) exhibited the highest acceleration, with 0.83 g in the tension and 0.64 g in the compression, and an average of 0.735 g in the experimental study, compared to 0.89 g in the analytical work. Duzce displayed the lowest acceleration for the BRB with TDA filling, with an average of 0.075 g in the tension and compression in the experimental study and 0.08 g in the analytical study.

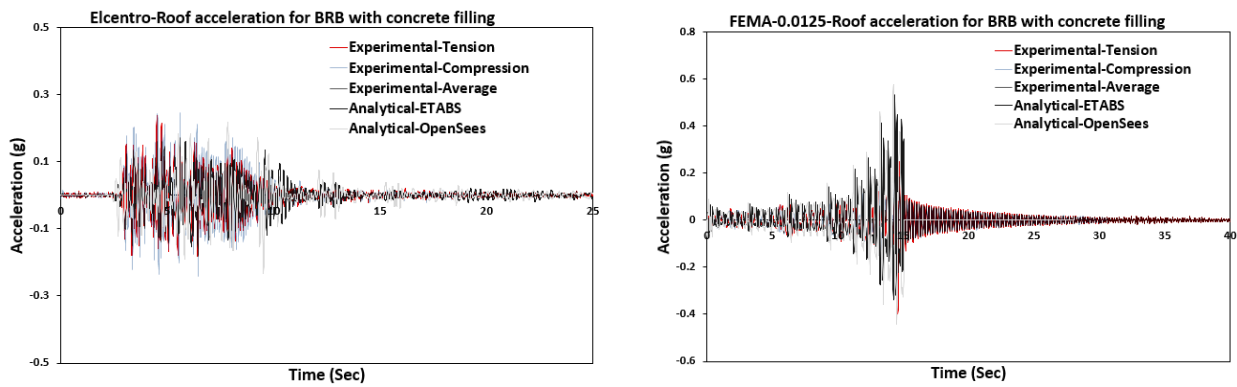


Figure 7. Comparison of roof acceleration for BRB with concrete filling subjected to different ground motions.

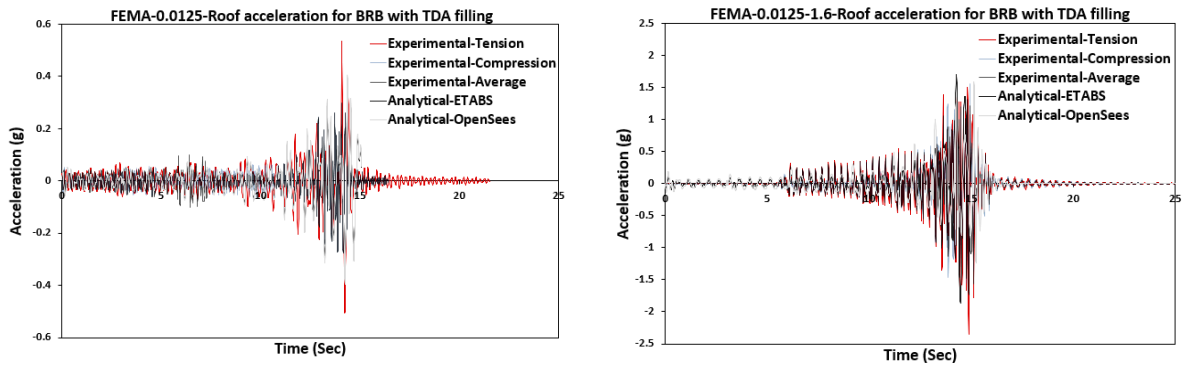


Figure 8. Comparison of roof acceleration for BRB with TDA filling subjected to different ground motions.

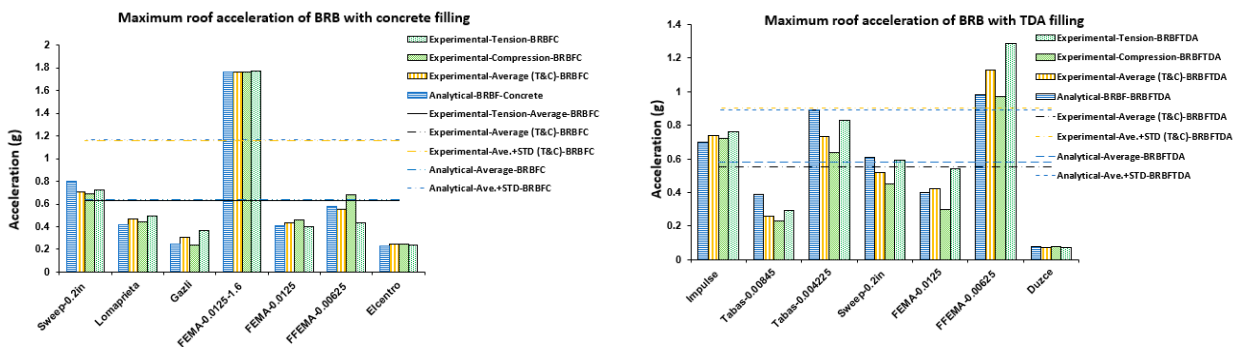


Figure 9. Selected maximum roof acceleration for BRB with concrete (left) and TDA filling (right).

Hysteresis loops of the BRB with TDA and concrete infills are presented in Figure 10. It is evident that the BRB with TDA infill dissipates less energy compared to the BRB with concrete infill. This observation aligns with the existing literature, indicating that the addition of rubber content in concrete mixtures leads to reduced flexural and compressive properties. A similar conclusion is drawn from the experimental work, which can be attributed to the unbinding of the rubber content within concrete mixtures.

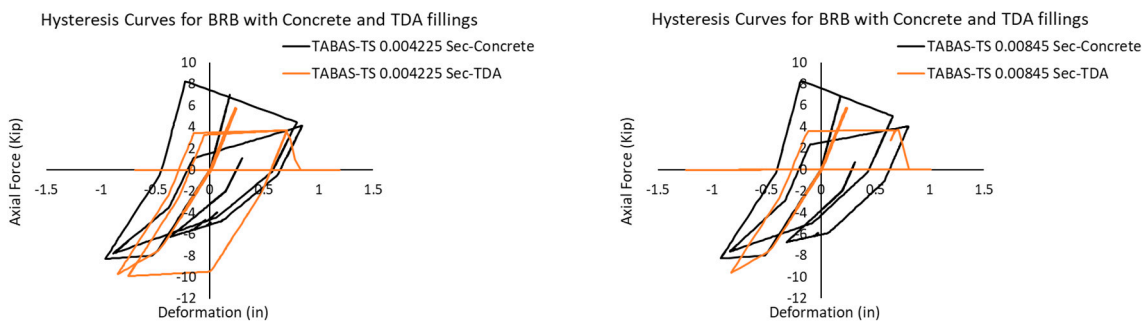


Figure 10. Results of hysteresis curves for BRB with TDA and concrete infills subjected to Tabas motion: TS-0.004225 (left), TS-0.00845 (right).

Figure 11 compares the backbone curves of the analytical and the experimental test for both BRB models with TDA and concrete fillings under FEMA 4 loading. The analytical and experimental results exhibit a consistent trend, revealing that the BRB with TDA filling is less ductile compared to the conventional concrete.

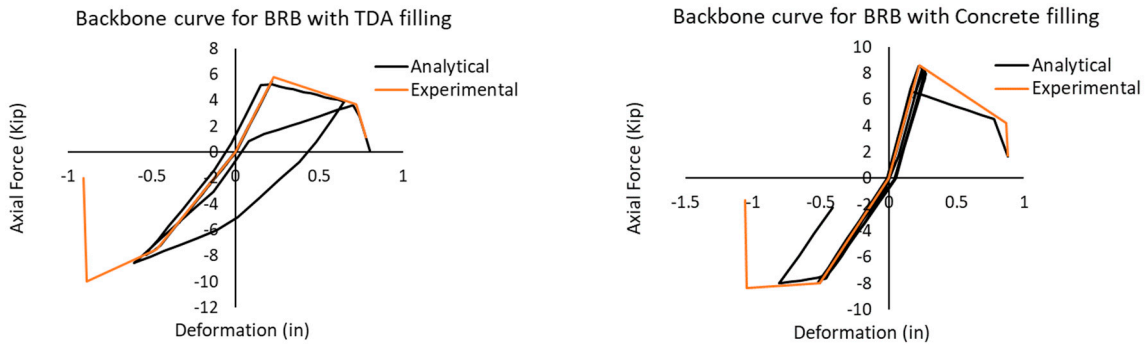


Figure 11. Comparison of hysteresis curves of analytical and experimental works for BRB with TDA (left) and with concrete filling (right).

The maximum roof displacements for the BRB with TDA and concrete infills are presented in Figure 12. The BRB frame with concrete infill showed the maximum roof displacements of 3.08 (in) in the tension and 2.97 (in) in the compression during the Gazli ground motion, with minimum roof displacements of 0.38 (in) and 0.28 (in) subjected to sweep loading. Analytically, the highest and lowest displacements were 2.75 (in) for the Gazali loading and 0.49 (in) for sweep loading. The BRB frame with TDA under the Tabas (TS-0.00845) ground motion had the maximum displacement of 2.67 (in) in the tension and 2.3 (in) in the compression for the experimental study, and 2.7 in the analytical work. The minimum roof displacement was 0.63 (in) in the tension and 0.43 (in) in the compression for the experimental frame, and 0.7 (in) for the simulated work under FEMA-0.0125 loading.

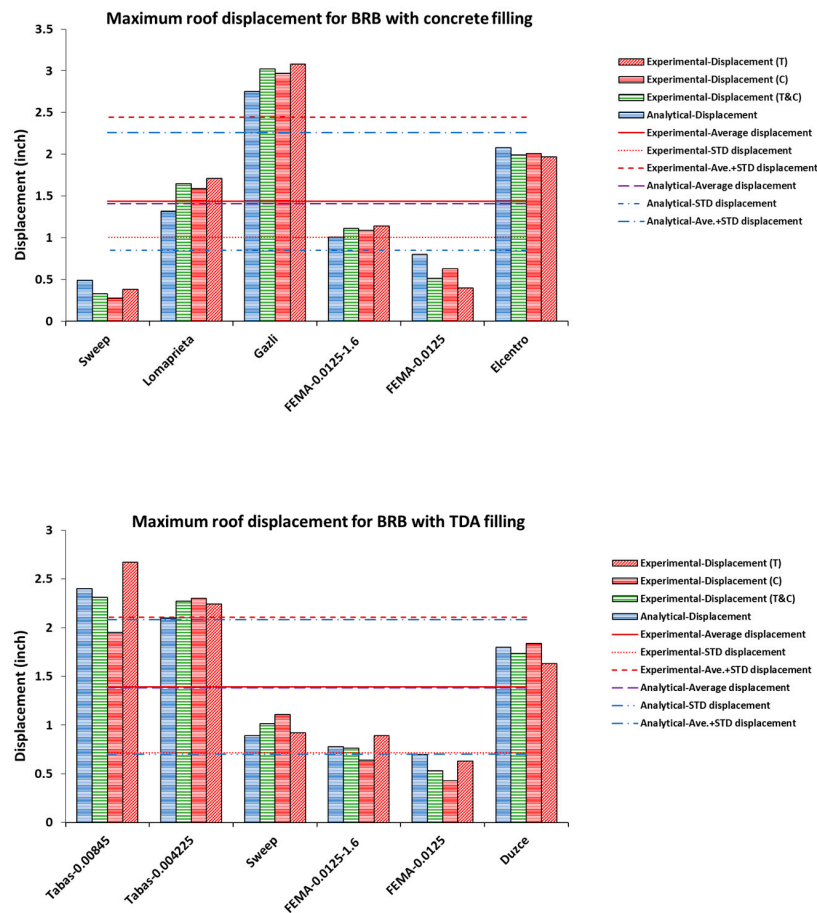


Figure 12. Maximum displacements for BRB with TDA and concrete fillings.

The effective stiffness is determined using a 1-inch impulse load, while system damping is derived from FEMA 4 loading based on the deformation response data. In both the experimental and analytical setting, the average effective stiffness of the BRB with concrete filling is 26.5 Kip/inch and 28 Kip/inch, respectively. For the BRB with TDA filling, the effective stiffness decreases to 20 Kip/inch in the experimental work and 21 Kip/inch in the analytical work. The damping ratios for the BRB with TDA filling exhibited a significant increase compared to the BRB with concrete infill, as shown in Table 3. The BRB with TDA demonstrated a notable 51% increase in damping compared to the conventional system.

Table 3. Buckling-restrained braced frame (BRBF)—damping ratio and stiffness (comparison of experimental and analytical results).

Description	Damping Ratio (%)			
	Experimental		Analytical	
	Tension	Compression	Tension	Compression
BRBF with TDA filling	16%	26%	25%	25%
BRBF with concrete filling	13%	17%	14%	14%
Description	Stiffness (Kip/in)			
	Experimental		Analytical	
	Tension	Compression	Tension	Compression
BRBF with TDA filling	19	21	21	21
BRBF with concrete filling	26	27	28	28

8. Design Guideline

ASCE 7 [41] establishes essential system design parameters, system-independent criteria, seismic hazard levels, redundancy, limitations, and conditions related to structural irregularities. AISC 341 [29] offers comprehensive design and detailing guidelines for individual structural elements, connections, and requirements to ensure the desired ductile behavior. In the context of a buckling-restrained braced frame (BRBF) system, the structure is expected to withstand significant inelastic deformation demands. Therefore, ASCE 7 [41] assigns the most prominent response modification coefficient ($R = 8$). The following steps and design procedures are recommended for a BRBF system with TDA infill:

The application of ductile tire-derived lightweight aggregate concrete significantly enhances the overall system performance. To achieve this, it is crucial to assess the mechanical properties of both the TDA and concrete including the compressive, flexural, and splitting tensile strength, toughness, and modulus of elasticity, among other important criteria, prior to the design process. This study relies on the experimental tests to determine these mechanical properties [15,16].

The reduction factors for buckling-restrained braced frames (BRBFs) depend on the building height and bracing configurations. To obtain more realistic results, it is recommended to calculate the response modification factor using pushover response curves [35]. However, in accordance with the current American code, ASCE 7 [41], BRBFs shall be designed based on the prescribed reduced reduction factor R . Then, select the appropriate load combinations.

The strength of the steel core can be defined as either the actual yield stress obtained from a coupon test or the specified minimum yield stress of the steel core. The design of the steel core must ensure its ability to resist axial forces within the brace [27].

The analysis and design of the BRB and control inelastic design level of the BRB strain and drift should adhere to the provisions outlined in AISC 341, ASCE 7, and ASCE 41 [29,35,41]. For the expected deformation, the greater value of either 0.02 times the story height (h_{sx}) or 2 times the story drift (Δ_x) should be considered.

Subsequently, the forces on the BRB are transferred to the connections, columns, and beams. Therefore, the design of the beams, columns, and connections should accommodate

the adjusted brace strength while remaining within the elastic zone. Additionally, all beam to column joints must guarantee sufficient shear strength to handle the extra forces from adjoining braces.

9. Conclusions

- This study compares experimental and analytical outcomes for a single-story steel frame utilizing buckling-restrained braces filled with TDA and concrete. It demonstrates the effectiveness of using tire-derived aggregates (TDAs) as an alternative material. It examines the innovative buckling-restrained brace with TDA infill, considering its potential for sustainability through reduced CO₂ emissions. A BRB with TDA contributes to sustainability and improves the damping properties compared to a conventional BRB with concrete infill. It provides numerical and experimental insights into structural responses, enhancing the existing knowledge. This study yields the following key conclusions:
- Analytical and experimental investigations on buckling-restrained braces (BRBs) with TDA infill have demonstrated a 25% increase in frame damping compared to a conventional BRB with a damping rate of approximately 14%. When higher damping is required, both the experimental and analytical findings suggest the use of a BRB with TDA infill. However, it is worth noting that a BRB with TDA filling offers a superior damping but reduced ductility compared to regular concrete, owing to the lower strength of TDA concrete, which cannot sufficiently delay steel core plate buckling as conventional concrete does [30].
- In general, a BRB with TDA filling reduced acceleration by approximately 20% compared to conventional concrete filling. The experimental study showed average acceleration values of 1.15 g with concrete and 0.91g with TDA fillings, while the analytical study results were 1.16 g with concrete and 0.89g with TDA fillings.
- The displacement value for the frame with the BRB and concrete infill was 2.44 (in) in the experimental and 2.26 (in) in the analytical study. Consequently, the BRB with TDA filling exhibits a lower ductility compared to the BRB with conventional concrete filling.
- A comparison of the hysteresis curves in both the analytical and experimental works revealed a similar trend in the backbone curves for the BRB with TDA and concrete infills subjected to FFEMA 4 loading. Furthermore, it was determined that the BRB with TDA infill absorbs less energy than the BRB with concrete infill, implying a lower ductility in the BRB with TDA infill compared to conventional concrete.

Additional experimental tests and numerical analyses in the future are necessary to fully understand the impact of a BRB with TDAFRC infill on the system performance. These studies may explore the potential for enhancing the ductility by incorporating fibers.

Author Contributions: Conceptualization, A.N., N.B.P. and L.C.; Methodology, A.N. and N.B.P.; Software, A.N.; Validation, A.N. and N.B.P.; Formal analysis, A.N.; Supervision, O.F. and F.M.T. All authors have read and agreed to the published version of the manuscript.

Funding: This research received no external funding.

Informed Consent Statement: Not applicable.

Data Availability Statement: Data are contained within the article.

Conflicts of Interest: The authors declare no conflict of interest.

References

1. Li, G.; Garrick, G.; Eggers, J.; Abadie, C.; Stubblefield, M.A.; Pang, S.-S. Waste Tire Fiber Modified Concrete. *Compos. Part B Eng.* **2004**, *35*, 305–312. [[CrossRef](#)]
2. Sukontasukkul, P. Use of Crumb Rubber to Improve Thermal and Sound Properties of Pre-Cast Concrete Panel. *Constr. Build. Mater.* **2009**, *23*, 1084–1092. [[CrossRef](#)]
3. Aslani, F. Mechanical Properties of Waste Tire Rubber Concrete. *J. Mater. Civ. Eng.* **2016**, *28*, 04015152. [[CrossRef](#)]

4. Ahn, I.S.; Cheng, L.; Fox, P.J.; Wright, J.; Patenaude, S.; Fujii, B. Material Properties of Large-Size Tire Derived Aggregate for Civil Engineering Applications. *J. Mater. Civ. Eng.* **2015**, *27*, 04014258. [[CrossRef](#)]
5. Ghaaowd, I.; McCartney, J.S.; Thielmann, S.S.; Sanders, M.J.; Fox, P.J. Shearing Behavior of Tire-Derived Aggregate with Large Particle Size. I: Internal and Concrete Interface Direct Shear. *J. Geotech. Geoenviron. Eng.* **2017**, *143*, 04017078. [[CrossRef](#)]
6. Mohammed, B.S.; Anwar Hossain, K.M.; Eng Swee, J.T.; Wong, G.; Abdullahi, M. Properties of Crumb Rubber Hollow Concrete Block. *J. Clean. Prod.* **2012**, *23*, 57–67. [[CrossRef](#)]
7. Topçu, I.B.; Avcular, N. Collision Behaviours of Rubberized Concrete. *Cem. Concr. Res.* **1997**, *27*, 1893–1898. [[CrossRef](#)]
8. Zheng, L.; Huo, X.S.; Yuan, Y. Strength, Modulus of Elasticity, and Brittleness Index of Rubberized Concrete. *J. Mater. Civ. Eng.* **2008**, *20*, 692–699. [[CrossRef](#)]
9. Atahan, A.O.; Sevim, U.K. Testing and Comparison of Concrete Barriers Containing Shredded Waste Tire Chips. *Mater. Lett.* **2008**, *62*, 3754–3757. [[CrossRef](#)]
10. Aiello, M.A.; Leuzzi, F. Waste Tyre Rubberized Concrete: Properties at Fresh and Hardened State. *Waste Manag.* **2010**, *30*, 1696–1704. [[CrossRef](#)]
11. Atahan, A.O.; Yücel, A.Ö. Crumb Rubber in Concrete: Static and Dynamic Evaluation. *Constr. Build. Mater.* **2012**, *36*, 617–622. [[CrossRef](#)]
12. Mohammed, B.S. Structural Behavior and m-k Value of Composite Slab Utilizing Concrete Containing Crumb Rubber. *Constr. Build. Mater.* **2010**, *24*, 1214–1221. [[CrossRef](#)]
13. Son, K.S.; Hajirasouliha, I.; Pilakoutas, K. Strength and Deformability of Waste Tyre Rubber-Filled Reinforced Concrete Columns. *Constr. Build. Mater.* **2011**, *25*, 218–226. [[CrossRef](#)]
14. Siddique, R.; Naik, T.R. Properties of Concrete Containing Scrap-Tire Rubber—An Overview. *Waste Manag.* **2004**, *24*, 563–569. [[CrossRef](#)] [[PubMed](#)]
15. Tehrani, F.M.; Miller, N.M. Tire-Derived Aggregate Cementitious Materials: A Review of Mechanical Properties. In *Cement Based Materials*; Saleh, H.E.-D.M., Rahman, R.O.A., Eds.; InTech: London, UK, 2018; ISBN 978-1-78984-153-4.
16. Tehrani, F.M.; Carreon, J.; Miller, N. An Investigation of Tire-Derived Lightweight Aggregate Concrete. *ACI Symp. Publ.* **2019**, *334*, 68–98. [[CrossRef](#)]
17. Treloar, L.R.G. Stress-Strain Data for Vulcanized Rubber under Various Types of Deformation. *Trans. Faraday Soc.* **1944**, *40*, 59–70. [[CrossRef](#)]
18. Wood, L.A. Uniaxial Extension and Compression in Stress-Strain Relations of Rubber. *J. Res. Natl. Bur. Stand.* **1977**, *82*, 57–63. [[CrossRef](#)] [[PubMed](#)]
19. Hertz, D.L., Jr. An analysis of rubber under strain from an engineering perspective. *J. Elastomerics* **1991**. Available online: <https://www.sealseastern.com/pdf/rubberunderstrain.pdf> (accessed on 2 November 2021).
20. Yang, H.; Jiang, L.; Zhang, Y.; Qi, P. Flexural Strength of Cement Paste Beam under Chemical Degradation: Experiments and Simplified Modeling. *J. Mater. Civ. Eng.* **2013**, *25*, 555–562. [[CrossRef](#)]
21. Toutanji, H.A. The Use of Rubber Tire Particles in Concrete to Replace Mineral Aggregates. *Cem. Concr. Compos.* **1996**, *18*, 135–139. [[CrossRef](#)]
22. Humphrey, D.; Blumenthal, M. The Use of Tire-Derived Aggregate in Road Construction Applications. In *Green Streets and Highways 2010*; American Society of Civil Engineers: Denver, CO, USA, 2010; pp. 299–313. [[CrossRef](#)]
23. CSI. Integrated Building Design Software, ETABS; *CSI Analysis Reference Manual, Computers and Structures*; Walnut Creek, CA, USA, 2016; Available online: <https://www.csiamerica.com/products/etabs> (accessed on 5 January 2021).
24. The Regents of the University of California. OpenSees User. 2000. Available online: https://opensees.berkeley.edu/wiki/index.php/OpenSees_User (accessed on 15 March 2021).
25. ASTM D6270; Standard Practice for Use of Scrap Tires in Civil Engineering Applications. ASTM: West Conshohocken, PA, USA, 2008. Available online: <https://www.astm.org/d6270-08.html> (accessed on 2 November 2021).
26. Miller, N.M.; Tehrani, F.M. Mechanical Properties of Rubberized Lightweight Aggregate Concrete. *Constr. Build. Mater.* **2017**, *147*, 264–271. [[CrossRef](#)]
27. Tehrani, F.M.; Masswadi, N.A.; Miller, N.M.; Sadrinezhad, A. An Experimental Investigation of Dynamic Properties of Fiber-Reinforced Tire-Derived Lightweight-Aggregate Concrete. *Eur. J. Eng. Technol. Res.* **2020**, *5*, 702–707. [[CrossRef](#)]
28. Kersting, R.A.; Fahnstock, L.A.; Lopez, W.A. *Seismic Design of Steel Buckling-Restrained Braced Frames: A Guide for Practicing Engineers*; National Institute of Standards and Technology: Gaithersburg, MD, USA, 2016; p. NIST GCR 15-917-34.
29. *ANSI/AISC 341*; Seismic Provisions for Structural Steel Buildings. American Institute of Steel Construction: Reston, VA, USA, 2016. Available online: <https://www.aisc.org/2016-Seismic-Provisions> (accessed on 5 November 2021).
30. Pathan, N.B.; Couch, L.; Tehrani, F.M.; Naghshineh, A.; Fischer, O. Experimental Seismic Evaluation of Novel Buckling-Restrained Braced Frames Containing Tire-Derived Aggregate Concrete. *Civ. Eng.* **2023**, *4*, 551–566. [[CrossRef](#)]
31. Naghshineh, A.; Tehrani, F.M.; Fischer, O. Application of Sustainable Concrete in the Seismic Evaluation of an Innovative Type of Buckling Restrained Brace. *Sustainability* **2022**, *14*, 16344. [[CrossRef](#)]
32. ASTM A36/A36M-19; Standard Specification for Carbon Structural Steel. ASTM International: West Conshohocken, PA, USA, 2019. [[CrossRef](#)]

33. Ancheta, T.D.; Darragh, R.B.; Stewart, J.P.; Seyhan, E.; Silva, W.J.; Chiou, B.S.J.; Wooddell, K.E.; Graves, R.W.; Kottke, A.R.; Boore, D.M.; et al. *PEER 2013/03—PEER NGA-West2 Database, PEER 2013/03*; Pacific Earthquake Engineering Research Center: Berkeley, CA, USA, 2013. Available online: <https://ngawest2.berkeley.edu> (accessed on 15 March 2021).
34. *FEMA 461*; Interim Testing Protocols for Determining the Seismic Performance Characteristics of Structural and Nonstructural Components. Federal Emergency Management Agency: Washington, CD, USA, 2007. Available online: <https://www.atcouncil.org/pdfs/FEMA461.pdf> (accessed on 15 March 2021).
35. *ASCE 41-17*; Seismic Evaluation and Retrofit of Existing Buildings (41-17). Available online: <https://sp360.asce.org/PersonifyEbusiness/Merchandise/Product-Details/productId/233163464> (accessed on 10 January 2021).
36. *FEMA P-2208*; NEHRP Recommended Revisions to ASCE/SEI 41-17, Seismic Evaluation and Retrofit of Existing Buildings. Available online: https://www.fema.gov/sites/default/files/documents/fema_p-2208.pdf (accessed on 10 January 2021).
37. McKenna, F. Object-Oriented Finite Element Programming: Frameworks for Analysis, Algorithms and Parallel Computing. Ph.D. Thesis, Civil Engineering, University of California, Berkeley, CA, USA, 1997.
38. McKenna, F.; Fenves, G.L.; Scott, M.H. *Open System for Earthquake Engineering Simulation*; University of California: Berkeley, CA, USA, 2000. Available online: <http://opensees.berkeley.edu> (accessed on 15 March 2021).
39. Mazzoni, S.; McKenna, F.; Scott, M.H.; Fenves, G.L. *OpenSees Command Language Manual*; University of California: Berkeley, CA, USA, 2006. Available online: <http://opensees.berkeley.edu/manuals/usermanual> (accessed on 15 March 2021).
40. McKenna, F.; Scott, M.H.; Fenves, G.L. Nonlinear finite-element analysis software architecture using object composition. *J. Comput. Civ. Eng.* **2010**, *24*, 95–107. [[CrossRef](#)]
41. *ASCE/SEI 7-22*; Minimum Design Loads and Associated Criteria for Buildings and Other Structures. American Society of Civil Engineers: Reston, VA, USA, 2022.

Disclaimer/Publisher’s Note: The statements, opinions and data contained in all publications are solely those of the individual author(s) and contributor(s) and not of MDPI and/or the editor(s). MDPI and/or the editor(s) disclaim responsibility for any injury to people or property resulting from any ideas, methods, instructions or products referred to in the content.